$T_e(R,t)$ measurements using electron Bernstein wave thermal emission on NSTX

S. J. Diem, G. Taylor, P. C. Efthimion, and B. P. LeBlanc
Princeton Plasma Physics Laboratory, P.O. Box 451, Princeton, New Jersey 08543

M. Carter, J. Caughman, and J. B. Wilgen
Oak Ridge National Laboratory, Fusion Energy Division, P.O. Box 2008, Oak Ridge, Tennessee 37831-6169

R. W. Harvey
CompX, Del Mar, California 92014

J. Preinhaelter and J. Urban
Czech Institute of Plasma Physics, Za Slovankou 3, 18200 Prague 8, Prague, Czech Republic

(Received 6 May 2006; presented on 9 May 2006; accepted 27 June 2006; published online 11 October 2006)

The National Spherical Torus Experiment (NSTX) routinely studies overdense plasmas with n_e of $(1-5)\times10^{19}$ m^{-3} and total magnetic field of <0.6 T, so that the first several electron cyclotron harmonics are overdense. The electrostatic electron Bernstein wave (EBW) can propagate in overdense plasmas, exhibits strong absorption, and is thermally emitted at electron cyclotron harmonics. These properties allow thermal EBW emission to be used for local T_e measurement. A significant upgrade to the previous NSTX EBW emission diagnostic to measure thermal EBW emission via the oblique *B-X-O* mode conversion process has been completed. The new EBW diagnostic consists of two remotely steerable, quad-ridged horn antennas, each of which is coupled to a dual channel radiometer. Fundamental (8–18 GHz) and second and third harmonic (18–40 GHz) thermal EBW emission and polarization measurements can be obtained simultaneously. © *2006 American Institute of Physics.* [DOI: 10.1063/1.2235112]

I. INTRODUCTION

A spherical torus[1] (ST) has low confining magnetic fields and high densities, so these devices typically have overdense plasmas that prohibit the use of electron cyclotron emission[2] (ECE) for localized temperature measurements. A plasma is considered overdense if it satisfies the condition $\omega_{pe}>n\Omega_{ce}$, where ω_{pe} is the angular electron plasma frequency, Ω_{ce} is the angular electron cyclotron frequency, and n is the harmonic number. The electrostatic electron Bernstein wave (EBW) can propagate in overdense plasmas while still exhibiting strong absorption at electron cyclotron harmonics. These properties allow thermal EBW emission to be used for a local T_e measurement in the ST. The National Spherical Torus Experiment[3] (NSTX) routinely studies overdense plasmas with n_e of $(1-5)\times10^{19}$ m^{-3} and total magnetic field of <0.6 T, so that the first several EC harmonics are overdense. Figure 1 shows a characteristic frequency plot versus major radius at the plasma midplane for an $I_p=800$ kA, $B_t(0)=4.5$ kG, helium *L*-mode NSTX plasma. The first five EC harmonics, upper hybrid resonance (UHR) layer, electron plasma frequency (*O*-mode cutoff), and right and left hand cutoffs are plotted in Fig. 1. The shaded regions in Fig. 1 represent the Doppler-broadened resonance location, $1/[1\pm3N_{\|}(v_T/c)]$, where typically $|N_{\|}|\sim\pm1$ (Ref. 4) near the emission location for NSTX plasmas, v_T is the electron thermal velocity, and c is the speed of light. Throughout the plasma $\omega_{pe}>n\Omega_{ce}$ $(n<5)$, prohibiting the use of ECE as a temperature diagnostic on NSTX. EBWs emitted near the EC resonance cannot propagate in a vacuum but can couple to the ordinary electromagnetic mode via the slow extraordinary mode (*B-X-O* mode conversion[5]) or can tunnel directly to the extraordinary electromagnetic mode (*B-X* mode conversion[6]). After mode conversion the emission then propagates into the vacuum region where it can be detected by an electromagnetic antenna and microwave heterodyne radiometry. Sweeping the radiometer detection frequency, and thus the EC resonance location, allows a radial profile measurement of EBW emission.

Previously, EBW conversion to *X*-mode emission (*B-X*) (Ref. 7) has been studied on NSTX, where a fixed antenna with a view normal to the plasma surface measured *B-X* mode conversion efficiencies up to 50% when a local limiter was used to enhance the *B-X* tunneling. The first *B-X-O* (Ref. 8) measurements on NSTX utilized a fixed quad-ridged horn antenna to measure fundamental emission from 8 to 18 GHz, yielding maximum mode conversion efficiencies of $80\%\pm20\%$. We report here details of new *B-X-O* emission diagnostic with two remotely steered antennas that have recently been installed on NSTX. This diagnostic measures thermal EBW emission in the 8–40 GHz frequency range, allowing the study of *B-X-O* mode conversion efficiency for fundamental, second, and third harmonic emissions. This new system may also provide a $T_e(R,t)$ diagnostic for NSTX.

The format of this article is as follows: Sec. II provides

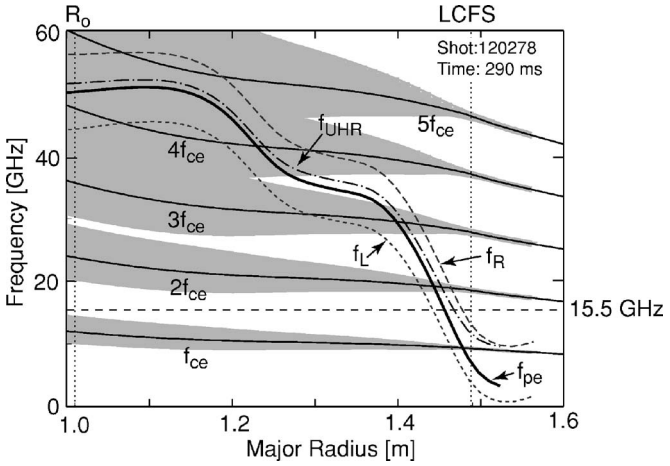

FIG. 1. The characteristic frequencies for an 800 kA, B_t=4.5 kG, helium *L*-mode NSTX plasma are plotted vs major radius on the plasma midplane. The first five electron cyclotron harmonics are plotted with thin solid lines. The shaded regions represent the Doppler-broadened resonance location for $n_{||}=\pm 1$. The vertical dashed line shows the location of the last closed flux surface. The thick solid line is the electron plasma frequency (*O*-mode cutoff) and the dashed-dotted line is the UHR frequency. *B-X-O* mode conversion occurs in the vicinity of these frequencies. The long and short dashed lines are the right and left hand cutoffs. Throughout most of the plasma the first four cyclotron harmonics are cutoff and not accessible by traditional ECE diagnostics.

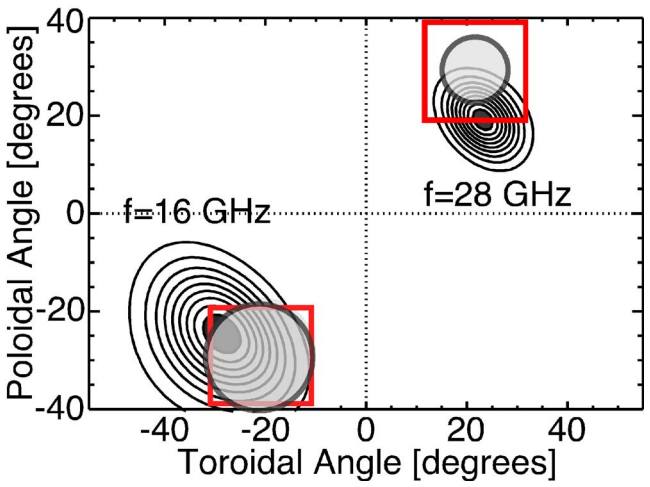

FIG. 2. (Color online) *B-X-O* mode conversion transmission function $T(n_\perp, n_{||})$ is shown for an 800 kA, B_t=4.5 kG, helium *H*-mode NSTX plasma for 16 GHz emission and 28 GHz emission. The 16 GHz emission corresponds to fundamental emission from near the plasma magnetic axis and the 28 GHz emission corresponds to second harmonic emission. The dark shaded regions represent >90% mode conversion efficiency. The lightly shaded circles represent the antenna beam waists near the upper hybrid resonance layer. The boxed areas indicate the regions the 8–18 and 18–40 GHz antennas can scan.

a brief description of EBW physics, Sec. III describes the newly installed EBW radiometer diagnostic on NSTX, and Sec. IV presents preliminary data obtained with the new diagnostic.

II. EBW PHYSICS

EBWs (Ref. 9) are electrostatic, hot plasma waves that propagate primarily perpendicular to the magnetic field and are emitted near electron cyclotron harmonics. The intensity of EBW radiation emitted from a plasma is given by[10]

$$I_\omega = \frac{\omega^2 k_B T_e}{8\pi^3 c^2}. \tag{1}$$

In Eq. (1), it is assumed that the plasma has an optical depth of $\tau > 2$ near the cyclotron resonance location to satisfy the blackbody condition. A plasma that is optically thick will emit EBWs with an intensity proportional to the local T_e. In NSTX, $\tau \sim 3000$ for emission near the electron cyclotron harmonics,[11] allowing EBW emission to be used as a $T_e(R,t)$ diagnostic.

Efficient *B-X-O* mode conversion can occur at oblique incidence to the magnetic field when the slow *X*-mode and *O*-mode cutoffs coincide. The angular transmission window for the *B-X-O* conversion process is given by[12,13]

$$T(n_\perp, n_{||}) = \exp\{-\pi k_o L_n \sqrt{(Y/2)}[2(1+Y)(n_{||,\mathrm{opt}} - n_{||})^2 + n_\perp^2]\}, \tag{2a}$$

$$n_{||,\mathrm{opt}}^2 = \left(\frac{Y}{Y+1}\right) = \cos^2(\phi_{\mathrm{opt}}), \tag{2b}$$

$$Y = \left(\frac{\Omega_{\mathrm{ce}}}{\omega}\right). \tag{2c}$$

In the equations above, Ω_{ce} and L_n are evaluated at the *O*-mode cutoff. The EBW emission can attain 100% conversion only when $n_{||}=n_{||,\mathrm{opt}}$ and $n_\perp=0$ which corresponds to oblique propagation at an angle ϕ_{opt} relative to the pure perpendicular propagation direction to the magnetic field at the cutoff. The optimal angle depends on the magnetic field strength and magnetic field pitch near the edge of the plasma. Decreasing the edge density scale length near the cutoff will result in a larger range of angles with >90% mode conversion efficiency. A calculation of the *B-X-O* transmission function $T(n_\perp, n_{||})$ is shown in Fig. 2 for an 800 kA NSTX plasma for emission at 16 GHz [fundamental emission near the core for $B_t(0)$=4.5 kG] and 28 GHz (second harmonic emission). The regions of >90% conversion efficiency are shaded in Fig. 2. The NSTX EBW diagnostic antenna system can scan in poloidal and toroidal angles to maximize *B-X-O* conversion efficiency. An additional prerequisite for efficient *B-X-O* mode conversion is that the EBW needs to also efficiently convert to the slow *X* mode at the UHR. We note that in a ST, as shown in Fig. 1, the *O*-mode cutoff and the UHR are normally located close together.

III. EBW EMISSION DIAGNOSTIC DESCRIPTION

An EBW emission radiometer system, consisting of two, two-channel heterodyne radiometers, has been installed on NSTX to simultaneously measure the fundamental (8–18 GHz) and second and third harmonic (18–40 GHz) EBW emissions from the plasma (Fig. 3). Each antenna is remotely steered by two linear drives mounted on each antenna (Fig. 4) to provide poloidal and toroidal steering corresponding to ±10° in the vacuum vessel (Fig. 2). The anten-

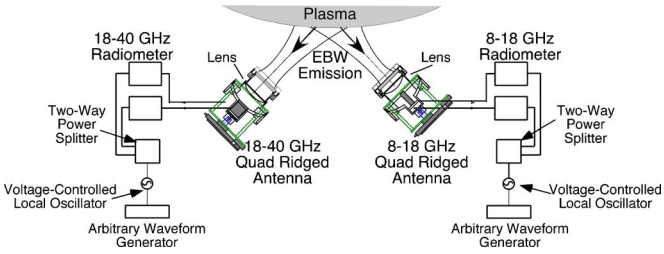

FIG. 3. (Color online) A schematic of dual antenna EBW emission diagnostic system is shown. This system is composed of two remotely steerable antennas coupled to a two-channel radiometer system.

nas, located outside the vacuum vessel, can be steered between plasma shots to optimize *B-X-O* conversion efficiency. Lenses in front of each antenna minimize the beam waist radius near the plasma edge (50 cm in front of the antennas) and, as a result, improve radial localization of T_e measurements with the diagnostic. The 8–18 GHz antenna (Tecom 201187-3 quad-ridged antenna) utilizes a 200 mm optical (100 mm microwave) focal length lens to provide a beam waist radius of 100 mm at the plasma edge for 16.5 GHz emission [shaded circle in Figs. 2 and 5(a)]. A 250 mm optical (125 mm microwave) focal length lens was used on the 18–40 GHz antenna (Q-Par WBH1840KDP quad-ridged antenna) to provide a beam waist radius of 65 mm at the plasma edge for 28 GHz emission [shaded circle in Figs. 2 and 5(b)].

The EBW emission power detected by each antenna is measured with two frequency scanning, heterodyne radiometers that measure orthogonal antenna polarization signals. An arbitrary wave form signal generator is used to drive a microwave voltage-controlled local oscillator (LO), General Microwave LO model V6120, for each heterodyne radiometer. Typically, the signal generator is programed to rapidly sweep the LO frequency allowing the diagnostic to scan in the EC resonance location, providing a $T_e(R,t)$ measurement. The signal generator is routinely swept linearly at 10 kHz, yielding scans of 100 μs. Maximum sweep rates of

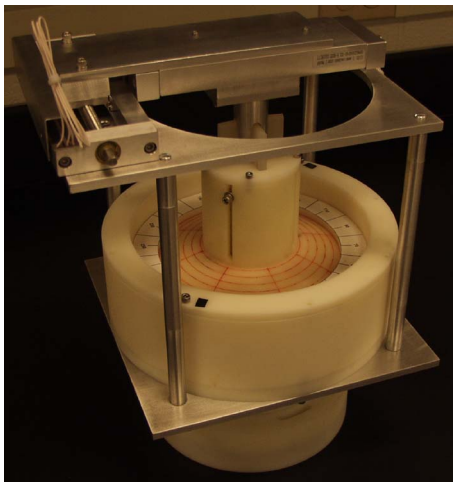

FIG. 4. (Color online) A picture of the antenna mounting fixture with the linear drives. The main antenna mounting fixture is manufactured out of nylon, allowing easy rotation on the hemisphere of nylon. The two linear drives mounted behind the antenna allow for movement of ±10° in the plasma in both the toroidal and poloidal directions.

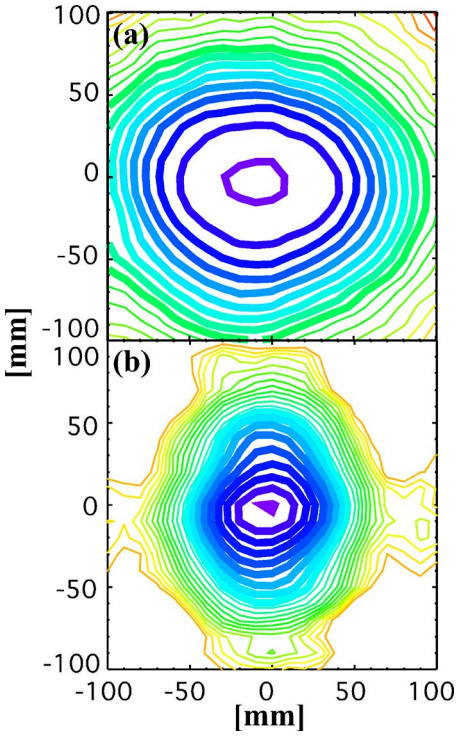

FIG. 5. (Color online) Antenna pattern for (a) 16.5 GHz and (b) 28 GHz measured 50 cm in front of the antennas, a distance typical of the separation between the antennas and the UHR layer. The bold lines represent the 9 dB spot size, or ~90% of the incident power. The beam waist radius for 16.5 GHz is 10 cm at the plasma edge while the beam waist radius for 28 GHz is 6.5 cm at the plasma edge.

100 kHz are possible. All of the radiometers were absolutely calibrated using a Dicke switching technique[14] incorporating the antennas and cabling used in the experiment. However, the vacuum window was not included during the calibration process and may provide 10%–20% decrease in the measured signal.

IV. PRELIMINARY DATA

Initial results from 8–40 GHz EBW emission diagnostic have recently been obtained for a helium *L*-mode, I_p=800 kA discharge. The preliminary frequency spectrum for the 8–18 GHz antenna is shown in Fig. 6. These preliminary results do not include an estimated 10%–20% correction for window loses. The fundamental emission peaks from 15 to 16 GHz during the current flattop, 0.25–0.4 s. The strong signal around 13.5 GHz (Fig. 6) is not EBW emission, but pickup from a nearby reflectometer source. Detailed three-dimensional (3D) EBW ray tracing and EBW emission simulations[4] will be employed to determine the *B-X-O* mode conversion efficiency, allowing the $T_e(R,t)$ profile to be measured from the evolution of the measured EBW emission spectrum. Experiments to study *B-X-O* mode conversion efficiency in *H*-mode plasmas in NSTX are planned for the near future.

V. DISCUSSION

A new *B-X-O* thermal EBW emission diagnostic is now operational on NSTX, providing fundamental, second, and

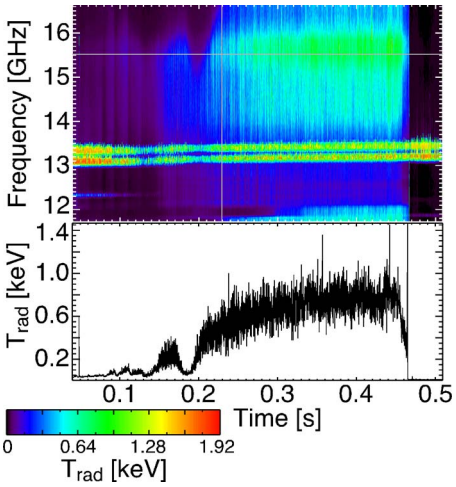

FIG. 6. (Color online) Preliminary data for 8–18 GHz antenna are shown in the contour plot. In the lower figure T_{rad} vs time is plotted for 15.5 GHz emission. The emission peaks during the plasma current flattop from 0.25 to 0.43 s.

third harmonic emission measurements from 8 to 40 GHz. Two remotely steered quad-ridged microwave horn antennas will allow detailed studies of *B-X-O* mode conversion physics and provide $T_e(R,t)$ measurements. Initial data have been taken to determine the mode conversion efficiency for a helium *L*-mode discharge and a peak in the emission has been observed. *B-X-O* emission modeling utilizing a 3D ray tracing and full wave code in the near future will provide a theoretical comparison for the experimental data to determine the mode conversion efficiency.

ACKNOWLEDGMENTS

The authors would like to thank Larry Guttadora for his technical support on this project. This research was supported by the United States Department of Energy Contract No. DE-AC02-76CH03073 and a grant to encourage innovations in fusion diagnostic systems.

[1] Y.-K. M. Peng and D. J. Strickler, Nucl. Fusion **26**, 769 (1986).
[2] M. Bornatici, Nucl. Fusion **23**, 1206 (1983).
[3] M. Ono *et al.*, Phys. Plasmas **4**, 799 (1997).
[4] J. Preinhaelter, J. Urban, P. Pavlo, V. Shevchenko, M. Valovic, L. Vanhala, and G. Vanhala, Rev. Sci. Instrum. **75**, 3804 (2004).
[5] J. Preinhaelter and V. Kopécky, J. Plasma Phys. **10**, 1 (1973).
[6] A. K. Ram and S. D. Schultz, Phys. Plasmas **7**, 4084 (2000).
[7] G. Taylor *et al.*, Phys. Plasmas **10**, 1395 (2003).
[8] G. Taylor *et al.*, Phys. Plasmas **12**, 052511 (2005).
[9] T. H. Stix, *Waves in Plasmas* (Springer, New York, 1992).
[10] G. Bekefi, *Radiation Processes in Plasmas* (Wiley, New York, 1966).
[11] P. C. Efthimion, J. C. Hosea, R. Kaita, R. Majeski, and G. Taylor, Rev. Sci. Instrum. **70**, 1018 (1999).
[12] E. Mjolhus, J. Plasma Phys. **31**, 7 (1984).
[13] F. R. Hansen, J. P. Lynoc, C. Maroli, and V. Petrillo, J. Plasma Phys. **39**, 319 (1988).
[14] R. H. Dicke, Rev. Sci. Instrum. **70**, 268 (1946).